



Critical behavior of the three-state random-field Potts model in three dimensions

Manoj Kumar ¹, Varsha Banerjee,² Sanjay Puri,³ and Martin Weigel ^{1,*}

¹*Institut für Physik, Technische Universität Chemnitz, 09107 Chemnitz, Germany*

²*Department of Physics, Indian Institute of Technology, Hauz Khas, New Delhi 110016, India*

³*School of Physical Sciences, Jawaharlal Nehru University, New Delhi 110067, India*



(Received 2 June 2022; accepted 12 October 2022; published 30 November 2022)

Enormous advances have been made in the past 20 years in our understanding of the random-field Ising model (RFIM), and there is now consensus on many aspects of its behavior at least in thermal equilibrium. In contrast, little is known about its generalization to the random-field Potts model (RFPM) which has wide-ranging applications. Here, we start filling this gap with an investigation of the three-state RFPM in three dimensions. Building on the success of ground-state calculations for the Ising system, we use a recently developed approximate scheme based on graph-cut methods to study the properties of the zero-temperature random fixed point of the system that determines the zero and nonzero temperature transition behavior. We find compelling evidence for a continuous phase transition. Implementing an extensive finite-size scaling analysis, we determine the critical exponents and compare them to those of the RFIM.

DOI: [10.1103/PhysRevResearch.4.L042041](https://doi.org/10.1103/PhysRevResearch.4.L042041)

I. INTRODUCTION

Understanding the effect of quenched disorder on phase transitions is crucial for many experiments, such as magnetic systems with impurities, and technological application areas, such as quantum computers [1]. At the same time, past progress in this direction has profoundly shaped the theory of equilibrium and nonequilibrium statistical mechanics, and theoretical concepts such as replica symmetry breaking and the cavity method have found applications even in seemingly distant fields such as gene regulation [2], neural networks [3], and the modeling of bird flocks [4].

Most of the recent focus has been on spin glasses, where competing and random interactions lead to a merely short-range ordered state, as well as on random-field systems [5]. The latter are at the heart of such diverse problems as the behavior of the quantum magnet $\text{LiHo}_x\text{Y}_{1-x}\text{F}_4$ [6] and the random first-order transition scenario in structural glasses [7,8]. For such problems, destruction of order is complete even for weak fields in $d = 2$ dimensions (2D) [9,10], where ferromagnetic domains break up on length scales that vanish with growing strength of the random fields [11]. For continuous $O(n)$ spins, the lower critical dimension is even elevated to $d_\ell = 4$. The random-field Ising model (RFIM), on the other hand, orders at nonzero temperatures already for $d \geq 3$, and the transition is of second order, at least for continuous field distributions [12–14]. Hence, the proposal of *dimensional reduction* [15] suggested by field theory, where the RFIM in d

dimensions would be in the universality class of the $d - 2$ -dimensional ferromagnet, does not apply in low dimensions but is only recovered for $d \geq d_c \approx 5$ [16–18].

Much less understood is the case of discrete spins with more than two states, i.e., the *random-field Potts model* (RFPM) [19,20]. The Potts model has a plethora of applications ranging from finite-temperature quantum chromodynamics [21], over mixed antiferromagnets [22], orientational glasses [23], to soap froths [24]. As disorder is inescapable, the RFPM is of even greater relevance for their study. Additionally, it is of profound theoretical interest since, in the pure Potts model [25], the transition order can be tuned by changing the number of states q , such that there is a line $q_c^{\text{pure}}(d)$ of tricritical points with $q_c^{\text{pure}}(2) = 4$ [26,27] and $q_c^{\text{pure}}(3) \approx 2.35$ [28]. Since disorder tends to soften first-order transitions [10,29], one expects a shift of the line $q_c^{\text{pure}}(d)$ to $q_c^{\text{RF}}(d)$. Just as for the RFIM, dimensional reduction is not likely to hold in low dimensions [20]. Instead, one expects [9,11] $d_\ell = 2$, and hence absence of long-range order in 2D—a scenario that we recently confirmed numerically [30]. A plausible behavior of $q_c^{\text{RF}}(d)$ is then $q_c^{\text{RF}}(d \rightarrow 2) \rightarrow \infty$ and $q_c^{\text{RF}} = 2$ for $d \geq 6$ [20,31]. Even once $q_c(d)$ is known, however, one needs to ask whether, for all strengths Δ of random fields, the first-order transition for $d_c^{\text{pure}}(q) \leq d \leq d_c^{\text{RF}}$ will be softened. This would be the case for $d = 2$ [10], but there is no ferromagnetic order there. In $d > 2$, one might expect a line of tricritical points (or even two lines [32]) to appear in the (Δ, T) plane, where the transition changes from first to second order [32,33].

Very little is known about the details of this rich phase diagram (but see Ref. [34]). The purpose of this Letter is to address such issues for the physically most relevant system of the $q = 3$, $d = 3$ RFPM, which in experiments has been used to describe trigonal-to-tetragonal structural transitions in SrTiO_3 [35] when stressed along [111], and the mixed antiferromagnet $\text{Fe}_{1-x}\text{Co}_x\text{Cl}_2$ [36]. Such experimental systems show

*martin.weigel@gmail.com

continuous transitions, but the theoretical situation is unclear as for this case $q_c^{\text{RF}} \geq q_c^{\text{pure}} \approx 2.35$. Some early simulational work [37] found first-order transitions for all considered field strengths, but later studies claimed a continuous transition for intermediate fields combined with first-order behavior for small and large fields [32,33]. This scenario agreed with the prediction of Ref. [20] but contradicted Ref. [38], which presented a $1/q$ expansion of the q -state RFPM in three dimensions (3D) and found a first-order transition for $q \geq 3$, irrespective of the field strength. The question of a softening of the discontinuous transition hence has remained undecided.

Due to frustration and the ensuing slow relaxation, Monte Carlo methods are not very efficient in the presence of random fields. For the RFIM, much of the recent progress in understanding is due to the availability of efficient combinatorial optimization methods that allow one to find exact ground states (GSs) in polynomial time [12,39–41]. Since the relevant renormalization-group fixed point is located at temperature $T = 0$, such GS calculations are also relevant for the finite-temperature transitions. Unfortunately, the same methods do not extend to the RFPM since the GS problem is NP hard for $q > 2$ [39,42]. As we have recently shown, however, combinatorial graph-cut methods [43,44] can still be used in combination with embedding techniques to efficiently compute high-quality approximate GSs [30,45]. To further improve the accuracy, we run the GS method for n different random initial spin configurations and extrapolate the thermodynamic quantities in the limit $n \rightarrow \infty$. The extrapolated results enable us to uncover a clear-cut picture of the phase transition.

II. MODEL AND METHODOLOGY

We consider the q -state RFPM with Hamiltonian [20]:

$$\mathcal{H} = -J \sum_{(ij)} \delta_{s_i, s_j} - \sum_i \sum_{\alpha=0}^{q-1} h_i^\alpha \delta_{s_i, \alpha}, \quad (1)$$

where $\delta_{x,y}$ is the Kronecker delta function, $s_i \in \{0, 1, \dots, q-1\}$, and $\{h_i^\alpha\}$ are uncorrelated, quenched random-field variables extracted from a standard normal distribution, i.e., $P(h_i^\alpha) = (2\pi\Delta^2)^{-1/2} \exp[-(h_i^\alpha)^2/(2\Delta^2)]$, and Δ denotes the disorder strength. For $q = 2$, Eq. (1) maps to the RFIM at coupling $J/2$ and field strength $\Delta/\sqrt{2}$ [30]. Note that different couplings of random fields to the spins are possible as well as different random-field distributions [31,32,34], but such variations are left for future work.

We perform GS calculations for the $q = 3$ RFPM on simple cubic lattices of edge length L with periodic boundary conditions. The number of disorder samples ranges from $N_{\text{samp}} = 50\,000$ for $L = 16$ to $N_{\text{samp}} = 5000$ for $L = 96$. Approximate GSs are obtained using the algorithm described in Ref. [30] that is based on an embedding of Ising spins into the Potts variables in the spirit of the α -expansion method of Ref. [42]. For each disorder sample, we run our algorithm for n different initial spin configurations and pick the run(s) resulting in the lowest energy as the GS estimate. The success probability of the resulting approach increases exponentially with n , such that the method becomes exact for $n \rightarrow \infty$ [45]. For each

sample, we determine the order parameter [25]:

$$m(L, \Delta, n) = \frac{q\rho - 1}{q - 1}, \quad \text{where } \rho = \frac{1}{L^3} \max_\alpha \sum_i \delta_{s_i, \alpha}. \quad (2)$$

Here, ρ denotes the density of spins in the majority orientation. Also, we measure the bond energy per spin $e_J(L, \Delta, n) = -\sum_{(ij)} \delta_{s_i, s_j}/L^3$ [46]. After performing the disorder average $[\cdot]_{\text{av}}$, we then deduce further quantities such as the Binder cumulant associated to m , $U_4(L, \Delta, n) = 1 - [m^4]_{\text{av}}/3[m^2]_{\text{av}}^2$. The employed definitions of the specific heat and magnetic susceptibility will be discussed below. All statistical errors were estimated using the jackknife method [47–49]. Estimates for Δ_c and the critical exponents are then extracted from the scaling of observables at sequences of pseudocritical points as well as from scaling collapses [50].

III. RESULTS

A. Extrapolation and transition order

To assess the quality of approximation, we first studied the behavior of each quantity as a function of n . We generally find a two-stage behavior, with an initial fast decay followed by a much slower large- n convergence, which is well described by the sum of two power laws [45]:

$$O(L, \Delta, n) = an^{-b}(1 + cn^{-e}) + O^*(L, \Delta), \quad (3)$$

where $b < e$ is the *asymptotic*, slow exponent, e describes the initial fast decay, and O^* denotes the limiting value for $n \rightarrow \infty$. As was shown elsewhere, this form is quite generic, and it holds particularly for a certain subset of samples for which exact GSs are known [45]. For such exact samples of size 16^3 , we employed our algorithm for up to $n = 10^4$ runs and found that the residuals with respect to the exact results, i.e., $O(n) - O_{\text{ex}}$ for any quantity scale as $an^{-b}(1 + cn^{-e})$, with $b \simeq 0.02$ and $e \simeq 0.5$. This behavior is seen to extend to the case where the exact results are not used or known [45]. The value of b is found to be very stable in this regard, such that we fix it for the subsequent fits of our main study reported here, for which $n \leq 100$ [51]. We then perform joint fits of the functional form in Eq. (3) to $[m]_{\text{av}}$, U_4 , and $[e_J]_{\text{av}}$ for a common value of the exponent e , yielding extrapolated estimates m^* , U^* , and e^* for any fixed (L, Δ) (see Sec. S1 in the Supplemental Material [52]). We prefix our analysis by a study of the energetic Binder cumulant, whose scaling clearly shows the behavior expected from a continuous transition, as already reported for $T > 0$ in Ref. [31]; details are provided in Sec. S2 in the Supplemental Material [52]. In the following, we perform finite-size scaling (FSS) of all quantities for finite n as well as for $n \rightarrow \infty$, to determine the transition point and obtain the critical exponents.

B. Magnetization and Binder cumulant

In Fig. 1(a), we show the extrapolated magnetization m^* as a function of the disorder strength Δ for various lattice sizes L . The expected FSS form [53]:

$$m^*(L, \Delta) = L^{-\beta/\nu} \widetilde{M}[(\Delta - \Delta_c)L^{1/\nu}], \quad (4)$$

implies that a plot of $m^*(L, \Delta)L^{\beta/\nu}$ against $x = (\Delta - \Delta_c)L^{1/\nu}$ should yield a collapse of datasets for small $|x|$ for appropriate

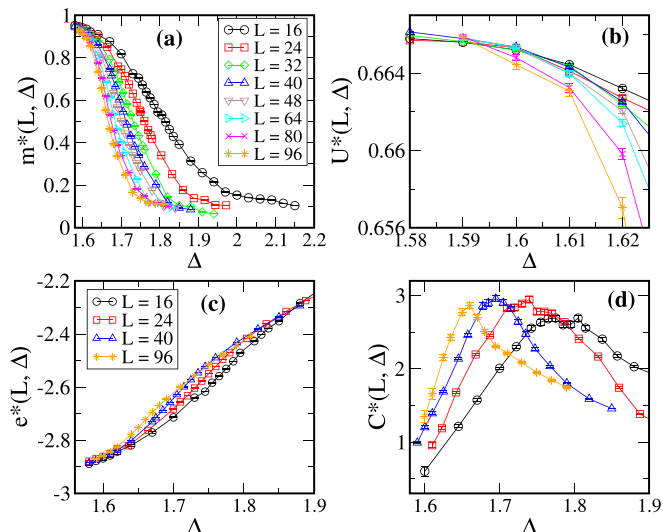


FIG. 1. Extrapolated estimates of the magnetization m^* , the Binder cumulant U^* , the bond energy e^* as well as the specific heat C^* as a function of Δ for various system sizes L .

values of Δ_c , ν , and β/ν . This is shown in Fig. 2(a). The collapse with the least mean-squared deviation S from the master curve [50,54] is obtained for $\Delta_c = 1.606 \pm 0.003$, $1/\nu = 0.723 \pm 0.004$, and $\beta/\nu = 0.0306 \pm 0.0023$. We also performed FSS of the magnetization for finite $n = 1, 5, 10, 50$, and 100. As is clear from Table I, there is a weak dependence of the estimates on n with a smooth convergence to the exact limit $n \rightarrow \infty$.

Turning to the Binder cumulant, from Fig. 1(b), we see a crossing of $U^*(L, \Delta) = U_4(L, \Delta, n \rightarrow \infty)$ in the range $\Delta_c = 1.59$ – 1.61 , predicting the location of the critical point, where U_4 becomes system-size independent [55,56]. The FSS form of U^* is [53] $U^*(L, \Delta) = \tilde{U}[(\Delta - \Delta_c)L^{1/\nu}]$. As is seen from the rescaled data in Fig. 2(b), a rather clean scaling collapse is achieved for $\Delta_c = 1.604(2)$ and $1/\nu = 0.720(6)$, yielding an alternative and consistent set of estimates for Δ_c and $1/\nu$.

C. Specific heat

Due to the restriction to $T = 0$ and the uniqueness of the GS, it is not possible to define the specific heat from a

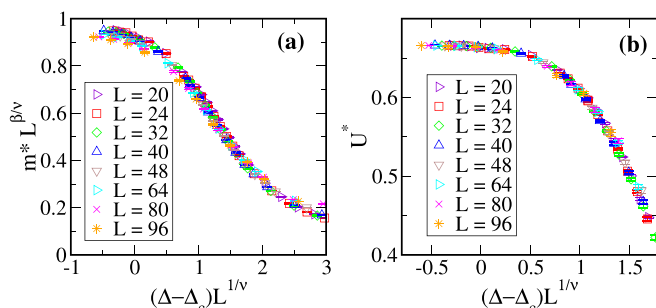


FIG. 2. (a) Scaling plot of $m^*(L, \Delta)L^{\beta/\nu}$ vs $(\Delta - \Delta_c)L^{1/\nu}$ with $\Delta_c = 1.606$, $1/\nu = 0.723$, and $\beta/\nu = 0.0306$. (b) Scaling collapse of U^* vs $(\Delta - \Delta_c)L^{1/\nu}$.

TABLE I. Estimates of Δ_c , ν , and β/ν according to Eq. (4) as well as $\tilde{\nu}/\nu$ according to Eq. (9) extracted from scaling collapses of the data for different n as well as the extrapolated data for $n \rightarrow \infty$ ($L_{\min} = 24$). S_1 and S_2 are the qualities of the collapses according to Eqs. (4) and (9), respectively ($S \approx 1$ for perfect collapses).

n	Δ_c	$1/\nu$	β/ν	$\tilde{\nu}/\nu$	S_1	S_2
1	1.636(2)	0.837(9)	0.0460(9)	2.9084(14)	2.30	2.38
5	1.626(3)	0.812(6)	0.0403(8)	2.9220(15)	1.82	1.69
10	1.623(5)	0.828(15)	0.0387(7)	2.9230(15)	1.28	1.58
50	1.617(4)	0.797(4)	0.0340(8)	2.9323(16)	1.25	1.38
100	1.616(1)	0.774(6)	0.0330(10)	2.9337(15)	1.20	1.36
∞	1.606(3)	0.723(4)	0.0306(23)	2.9402(30)	0.82	0.87

temperature derivative or fluctuation-dissipation relation. Instead, a specific-heat-like quantity is given by the derivative $C(\Delta) = \partial[e_r(\Delta)]_{\text{av}}/\partial\Delta$ [46,57]. Numerically, we compute this using the standard three-point formula at the midpoint [58]. In Fig. 1(d), we show the extrapolated $C^*(L, \Delta)$. As L is increased, the peaks shift but only weakly vary in height, indicating a small specific heat exponent α . To determine the latter, we considered additional Δ values and used parabolic fits $C(L, \Delta) = a_0(\Delta - \Delta_{\max,C})^2 + C_{\max}$ to obtain the peak locations $\Delta_{\max,C}(L)$ and peak heights $C_{\max}(L)$. In a finite system, the singular part of $C(L, \Delta)$ scales as [53] $C_s(L, \Delta) = L^{\alpha/\nu} \tilde{C}[(\Delta - \Delta_c)L^{1/\nu}]$. If the maximum of \tilde{C} occurs for argument a_1 , then the positions in Δ shift as

$$\Delta_{\max,C}(L) \approx \Delta_c + a_1 L^{-1/\nu}, \quad (5)$$

and the maximum value of the singular part of the specific heat $C_{s,\max}(L) \sim L^{\alpha/\nu}$.

Figure 3(a) shows our data for $\Delta_{\max,C}(L)$ together with fits of the form in Eq. (5), indicating clear consistency. The estimates of Δ_c and the exponent $1/\nu$ are collected in Table II, where we also indicate the quality Q_1 of these fits [58]. In Fig. 3(b), we present the corresponding peak heights $C_{\max}(L, n)$. This plot clearly suggests that α is either positive but very small or negative. As a consequence, scaling corrections are relevant, and we hence considered the functional

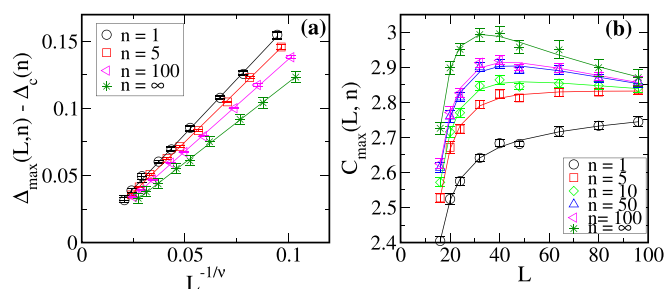


FIG. 3. (a) Shifts $\Delta_{\max,C}(L) - \Delta_c$ of the pseudocritical fields of the specific heat against $L^{-1/\nu}$ for different n , where Δ_c and the exponent $1/\nu$ are determined from fits of the form in Eq. (5), see Table II. For increased clarity, the data for different n are slightly shifted relative to each other. (b) Scaling of the maxima $C_{\max}(L)$ as a function of L for different n . The curves correspond to fits of the form in Eq. (6) to the data (cf. Table II).

TABLE II. Parameters of fits of the functional forms in Eqs. (5) and (6) to the data for the specific heat. Q_1 and Q_2 refer to the quality of fit [58].

n	Δ_c	$1/\nu$	α/ν	ω	Q_1	Q_2
1	1.644(6)	0.850(70)	0.023(12)	2.67(87)	0.74	0.71
5	1.626(3)	0.774(32)	-0.002(11)	2.62(68)	0.32	0.70
10	1.621(3)	0.767(25)	-0.019(13)	2.39(61)	0.14	0.52
50	1.620(2)	0.776(21)	-0.046(20)	1.87(53)	0.12	0.50
100	1.620(2)	0.780(21)	-0.049(20)	1.86(52)	0.15	0.49
∞	1.611(4)	0.733(28)	-0.059(20)	2.52(73)	0.14	0.93

form:

$$C_{\max}(L) = C_0 + c_1 L^{\alpha/\nu} (1 + c_2 L^{-\omega}), \quad (6)$$

where ω corresponds to the Wegner exponent, and C_0 represents a nonsingular background term. Since $\alpha \approx 0$ effectively results in a second additive constant in Eq. (6), we cannot reliably include all five parameters in the fit. We hence fix $C_0 = 0$, and the resulting four-parameter fit yields excellent qualities Q_2 and the estimates of α/ν and ω collected in Table II. We thus conclude that α is very slightly negative or perhaps zero.

D. Susceptibility

We now turn to the connected and disconnected magnetic susceptibilities. Since we operate at $T = 0$, we cannot use the usual fluctuation-dissipation relation. As outlined in Sec. S3 in the Supplemental Material [52], we generalize arguments for the RFIM [59] to express the zero-field RFPM susceptibility:

$$\left[\frac{\partial \langle M^\mu \rangle}{\partial H^\mu} \right]_{\text{av}} = \int d\{\bar{h}_i^\alpha\} P(\{\bar{h}_i^\alpha\}) \frac{\partial \langle M^\mu \rangle_{\bar{h}_i^\alpha}}{\partial H^\mu}, \quad (7)$$

for Gaussian random fields as $\chi^\mu = [\langle m^\mu \rangle \sum_i h_i^\mu]_{\text{av}} / \Delta^2$, where $m^\mu = \sum_i \delta_{s_i, \mu} / L^3$ (see also Ref. [13]). We apply a constant external field H to the spin state 1 (i.e., $\mu = 1$) to break the symmetry so that χ displays a peak. As is shown in Sec. S3 in the Supplemental Material [52], a minimal field strength $\propto L^{-3/2}$ is necessary to break the symmetry, and we choose $H(L = 16) = 8 \times 10^{-2}$. Due to the large sample-to-sample fluctuations in χ , we do not observe a systematic variation of $\chi(L, \Delta, n)$ with n , such that, instead of an extrapolation, we focus on $n = 100$. Figure 4(a) shows the behavior of $\chi(L, \Delta, n = 100)$ as a function of Δ and for various L . To analyze its divergence, we fit a parabola near the peak and obtain the peak positions $\Delta_{\max, \chi}(L)$ as well as the maxima of the susceptibility $\chi_{\max}(L)$. FSS predicts that

$$\chi(L, \Delta) = L^{\gamma/\nu} \tilde{\chi}[(\Delta - \Delta_c) L^{1/\nu}], \quad \chi_{\max}(L) \sim L^{\gamma/\nu}. \quad (8)$$

A power law fit of the form in Eq. (8) for $\chi_{\max}(L)$ yields $\gamma/\nu = 1.36(1)$ ($Q = 0.034$). Similarly, using the form $\Delta_{\max, \chi}(L) = \Delta_c + a_1 L^{-1/\nu}$ for the peak locations yields the estimates $\Delta_c = 1.621(5)$ and $1/\nu = 0.97(5)$ ($Q = 0.007$). The corresponding data are shown in Fig. S5(a) in the Supplemental Material [52]. While the value of Δ_c agrees with that obtained from the specific heat (see Table II for

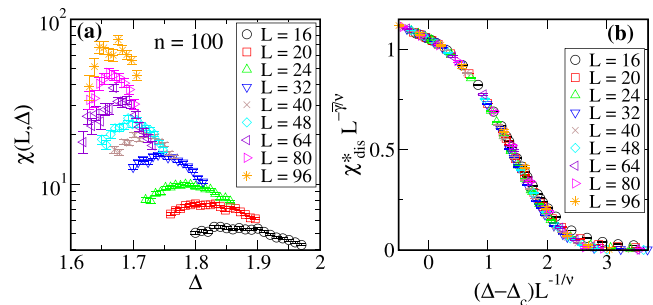


FIG. 4. (a) $\chi(L, \Delta, n = 100)$ (on a log-linear scale) against Δ and for different L (see key). (b) Data collapse of $\chi_{\text{dis}}^*(L, \Delta)$ with the exponent values in Table I.

$n = 100$), the estimate for $1/\nu$ is noticeably larger than the values from the magnetization and specific heat, indicative of unresolved scaling corrections. To avoid this problem, we performed additional simulations without external field H at fixed $\Delta \in [1.602, 1.606]$, corresponding to the estimate $\Delta_c = 1.604(2)$ found above from $U^*(L, \Delta)$. Here, we find clean scaling, cf. Fig. S5(b) in the Supplemental Material [52], and the fit parameters are collected in Table S1 in the Supplemental Material [52], indicating little scaling corrections in χ , and the dependence of γ/ν on Δ is only weak; we quote $\gamma/\nu = 1.51(6)$ at our best estimate $\Delta_c = 1.604$ for $L_{\min} = 16$.

The additional length scale introduced by the disorder fluctuations results in a different scaling behavior of the static, disconnected susceptibility $\chi_{\text{dis}} = L^d [m^2]_{\text{av}}$ as compared to the thermal, connected susceptibility χ [60]:

$$\chi_{\text{dis}}(L, \Delta) = L^{\tilde{\gamma}/\nu} \tilde{\chi}_{\text{dis}}[(\Delta - \Delta_c) L^{1/\nu}]. \quad (9)$$

We use this relation to perform a scaling collapse for the extrapolated χ_{dis}^* . As is shown in Fig. 4(b), this leads to an excellent scaling result; the exponents $\tilde{\gamma}/\nu$, including those for finite n , are provided in Table I, with $\tilde{\gamma}/\nu = 2.9402(30)$ for $n = \infty$. The so-called two-exponent scaling scenario predicts $\tilde{\gamma} = 2\gamma$ [61,62]. From our data, we find the marginal result $(2\gamma - \tilde{\gamma})/\nu = 0.08(6)$. We can also investigate the validity of the Rushbrooke equality $\alpha + 2\beta + \gamma = 2$ and the modified hyperscaling relation $2 - \alpha = \nu(d - \theta)$ [60,63,64], where $\theta = 2 - \bar{\eta} + \eta = (\tilde{\gamma} - \gamma)/\nu$. It can be inspected from Tables I and II that both relations are well satisfied (within error bars) by the results for infinite n .

IV. CONCLUSIONS

We have presented a high-resolution numerical study of the 3D three-state RFPM via a computationally efficient GS method that uses extrapolation in the number n of initial conditions to provide quasi-exact results. With the help of FSS, all critical exponents, including the most elusive specific heat exponent α , are determined for finite as well as infinite n , providing clear evidence for a continuous phase transition in the vicinity of $\Delta_c = 1.604(2)$. Given that we are working at $T = 0$, it is hence clear that $3 = q < q_c^{\text{RF}}(3)$. We have thus provided a comprehensive calculation of critical exponents. As the summary in Table III shows, these

TABLE III. Critical exponents of the 3D $q = 3$ RFPM as compared with those of the RFIM [16].

	RFIM	$q = 3$ RFPM
ν	1.38(10)	1.383(8)
α	-0.16(35)	-0.082(28)
β	0.019(4)	0.0423(32)
γ	2.05(15)	2.089(84)
η	0.5139(9)	0.49(6)
$\bar{\eta}$	1.028(2)	1.060(3)
θ	1.487(1)	1.43(6)
$\alpha + 2\beta + \gamma$	2.00(31)	2.08(9)

are close to but likely distinct from the exponents of the 3D RFIM [12,40]. It will be most interesting to see if

this deviation grows stronger as q is increased to four and possibly beyond and if and when the transition turns first order.

ACKNOWLEDGMENTS

We thank N. Fytas for a careful reading of the manuscript. The authors are thankful to Kurt Binder for manifold discussions on topics related to the manuscript. M.K. and M.W. acknowledge the support of the Royal Society–SERB Newton International fellowship (NIF\R1\180386). All numerical simulations were done on the parallel compute cluster *Zeus* of Coventry University. The publication of this Letter was funded by Chemnitz University of Technology and by the Deutsche Forschungsgemeinschaft under Project No. 491193532.

- [1] S. Boixo, T. F. Ronnow, S. V. Isakov, Z. Wang, D. Wecker, D. A. Lidar, J. M. Martinis, and M. Troyer, Evidence for quantum annealing with more than one hundred qubits, *Nat. Phys.* **10**, 218 (2014).
- [2] A. Decelle, F. Krzakala, C. Moore, and L. Zdeborová, Inference and Phase Transitions in the Detection of Modules in Sparse Networks, *Phys. Rev. Lett.* **107**, 065701 (2011).
- [3] H. Nishimori, *Statistical Physics of Spin Glasses and Information Processing* (Oxford University Press, Oxford, 2001).
- [4] W. Bialek, A. Cavagna, I. Giardina, T. Mora, E. Silvestri, M. Viale, and A. M. Walczak, Statistical mechanics for natural flocks of birds, *Proc. Natl. Acad. Sci. USA* **109**, 4786 (2012).
- [5] *Spin Glasses and Random Fields*, edited by A. P. Young (World Scientific, Singapore, 1997).
- [6] D. Silevitch, D. Bitko, J. Brooke, S. Ghosh, G. Aeppli, and T. Rosenbaum, A ferromagnet in a continuously tunable random field, *Nature (London)* **448**, 567 (2007).
- [7] X. Xia and P. G. Wolynes, Fragilities of liquids predicted from the random first order transition theory of glasses, *Proc. Natl. Acad. Sci. USA* **97**, 2990 (2000).
- [8] B. Guiselin, L. Berthier, and G. Tarjus, Random-field Ising model criticality in a glass-forming liquid, *Phys. Rev. E* **102**, 042129 (2020).
- [9] J. Z. Imbrie, Lower Critical Dimension of the Random-Field Ising Model, *Phys. Rev. Lett.* **53**, 1747 (1984).
- [10] M. Aizenman and J. Wehr, Rounding of First-Order Phase Transitions in Systems with Quenched Disorder, *Phys. Rev. Lett.* **62**, 2503 (1989).
- [11] K. Binder, Random-field induced interface widths in Ising systems, *Z. Phys. B* **50**, 343 (1983).
- [12] N. G. Fytas and V. Martín-Mayor, Universality in the Three-Dimensional Random-Field Ising Model, *Phys. Rev. Lett.* **110**, 227201 (2013).
- [13] N. G. Fytas, V. Martín-Mayor, M. Picco, and N. Sourlas, Phase Transitions in Disordered Systems: The Example of the Random-Field Ising Model in Four Dimensions, *Phys. Rev. Lett.* **116**, 227201 (2016).
- [14] M. Kumar, V. Banerjee, and S. Puri, Random field Ising model in a uniform magnetic field: Ground states, pinned clusters and scaling laws, *Eur. Phys. J. E* **40**, 96 (2017).
- [15] A. Aharony, Y. Imry, and S.-k. Ma, Lowering of Dimensionality in Phase Transitions with Random Fields, *Phys. Rev. Lett.* **37**, 1364 (1976).
- [16] N. G. Fytas, V. Martín-Mayor, M. Picco, and N. Sourlas, Restoration of dimensional reduction in the random-field Ising model at five dimensions, *Phys. Rev. E* **95**, 042117 (2017).
- [17] M. Tissier and G. Tarjus, Supersymmetry and Its Spontaneous Breaking in the Random Field Ising Model, *Phys. Rev. Lett.* **107**, 041601 (2011).
- [18] A. Kaviraj, S. Rychkov, and E. Trevisani, Parisi-Sourlas Supersymmetry in Random Field Models, *Phys. Rev. Lett.* **129**, 045701 (2022).
- [19] H. Nishimori, Potts model in random fields, *Phys. Rev. B* **28**, 4011 (1983).
- [20] D. Blankshtein, Y. Shapir, and A. Aharony, Potts models in random fields, *Phys. Rev. B* **29**, 1263 (1984).
- [21] M. Alford, S. Chandrasekharan, J. Cox, and U.-J. Wiese, Solution of the complex action problem in the Potts model for dense QCD, *Nucl. Phys. B* **602**, 61 (2001).
- [22] E. Domany, Y. Shnidman, and D. Mukamel, Type I FCC antiferromagnets in a magnetic field: A realisation of the $q = 3$ - and $q = 4$ -state Potts models, *J. Phys. C* **15**, L495 (1982).
- [23] K. Binder and J. Reger, Theory of orientational glasses: Models, concepts, simulations, *Adv. Phys.* **41**, 547 (1992).
- [24] F. Graner and J. A. Glazier, Simulation of Biological Cell Sorting Using a Two-Dimensional Extended Potts Model, *Phys. Rev. Lett.* **69**, 2013 (1992).
- [25] F. Y. Wu, The Potts model, *Rev. Mod. Phys.* **54**, 235 (1982).
- [26] H. Duminil-Copin, V. Sidoravicius, and V. Tassion, Continuity of the phase transition for planar random-cluster and Potts models with $1 \leq q \leq 4$, *Commun. Math. Phys.* **349**, 47 (2017).
- [27] H. Duminil-Copin, M. Gagnebin, M. Harel, I. Manolescu, and V. Tassion, Discontinuity of the phase transition for the planar random-cluster and Potts models with $q > 4$, *Ann. Sci. Ec. Norm. Super.* **54**, 1363 (2021).
- [28] A. K. Hartmann, Calculation of Partition Functions by Measuring Component Distributions, *Phys. Rev. Lett.* **94**, 050601 (2005).
- [29] J. Cardy, Quenched randomness at first-order transitions, *Physica A* **263**, 215 (1999).

- [30] M. Kumar, R. Kumar, M. Weigel, V. Banerjee, W. Janke, and S. Puri, Approximate ground states of the random-field Potts model from graph cuts, *Phys. Rev. E* **97**, 053307 (2018).
- [31] K. Eichhorn and K. Binder, Monte Carlo investigation of the three-dimensional random-field three-state Potts model, *J. Phys.: Condens. Matter* **8**, 5209 (1996).
- [32] K. Eichhorn and K. Binder, Finite-size scaling study of the three-state Potts model in random fields: Evidence for a second-order transition, *Europhys. Lett.* **30**, 331 (1995).
- [33] K. Eichhorn and K. Binder, The three-dimensional three-state Potts ferromagnet exposed to random fields: evidence for a second order transition, *Z. Phys. B - Condensed Matter* **99**, 413 (1995).
- [34] A. Türkoğlu and A. N. Berker, Phase transitions of the variety of random-field Potts models, *Physica A* **583**, 126339 (2021).
- [35] A. Aharony, K. Müller, and W. Berlinger, Trigonal-To-Tetragonal Transition in Stressed SrTiO₃: A Realization of the Three-State Potts Model, *Phys. Rev. Lett.* **38**, 33 (1977).
- [36] D. Mukamel, Phase Diagrams and Multicritical Points in Randomly Mixed Alloys, *Phys. Rev. Lett.* **46**, 845 (1981).
- [37] P. Reed, The Potts model in a random field: A Monte Carlo study, *J. Phys. C: Solid State Phys.* **18**, L615 (1985).
- [38] Y. Y. Goldschmidt and G. Xu, Phase diagrams of the random-field Potts model in three dimensions, *Phys. Rev. B* **32**, 1876 (1985); The random-field Potts model in three dimensions, *Nucl. Phys. B* **265**, 1 (1986).
- [39] J. A. d'Auriac, M. Preissmann, and R. Rammal, The random field Ising model: Algorithmic complexity and phase transition, *J. Phys. Lett.* **46**, 173 (1985).
- [40] A. A. Middleton and D. S. Fisher, Three-dimensional random-field Ising magnet: Interfaces, scaling, and the nature of states, *Phys. Rev. B* **65**, 134411 (2002).
- [41] J. D. Stevenson and M. Weigel, Domain walls and Schramm-Loewner evolution in the random-field Ising model, *Europhys. Lett.* **95**, 40001 (2011).
- [42] Y. Boykov, O. Veksler, and R. Zabih, Fast approximate energy minimization via graph cuts, *IEEE Trans. Pattern Anal. Machine Intell.* **23**, 1222 (2001).
- [43] V. Kolmogorov and R. Zabih, What energy functions can be minimized via graph cuts? *IEEE Trans. Pattern Anal. Machine Intell.* **26**, 147 (2004).
- [44] Y. Boykov and V. Kolmogorov, An experimental comparison of min-cut/max-flow algorithms for energy minimization in vision, *IEEE Trans. Pattern Anal. Machine Intell.* **26**, 1124 (2004).
- [45] M. Kumar and M. Weigel, Quasi-exact ground-state algorithm for the random-field Potts model, [arXiv:2204.11745](https://arxiv.org/abs/2204.11745).
- [46] A. K. Hartmann and A. P. Young, Specific-heat exponent of random-field systems via ground-state calculations, *Phys. Rev. B* **64**, 214419 (2001).
- [47] B. Efron, *The Jackknife, the Bootstrap and Other Resampling Plans* (SIAM, Philadelphia, 1982).
- [48] R. G. Miller, The jackknife—a review, *Biometrika* **61**, 1 (1974).
- [49] M. Weigel and W. Janke, Error estimation and reduction with cross correlations, *Phys. Rev. E* **81**, 066701 (2010).
- [50] O. Melchert, autoScale.py—a program for automatic finite-size scaling analyses: A user's guide, [arXiv:0910.5403](https://arxiv.org/abs/0910.5403).
- [51] We have explicitly verified that a slight variation in the exponent b does not yield significantly different results in the extrapolations.
- [52] See Supplemental Material at <http://link.aps.org/supplemental/10.1103/PhysRevResearch.4.L042041> for details regarding the extrapolation for physical quantities, the order of the transition, and the fluctuation formula for the susceptibility.
- [53] V. Privman, Finite-size scaling theory, in *Finite Size Scaling and Numerical Simulation of Statistical Systems*, edited by V. Privman (World Scientific, Singapore, 1990), pp. 1–98.
- [54] J. Houdayer and A. K. Hartmann, Low-temperature behavior of two-dimensional gaussian Ising spin glasses, *Phys. Rev. B* **70**, 014418 (2004).
- [55] K. Binder, Finite size scaling analysis of Ising model block distribution functions, *Z. Phys. B* **43**, 119 (1981).
- [56] K. Binder and D. W. Heermann, *Monte Carlo Simulation in Statistical Physics*, 5th ed. (Springer-Verlag, Berlin, Heidelberg, 2010).
- [57] N. G. Fytas, P. E. Theodorakis, and A. K. Hartmann, Revisiting the scaling of the specific heat of the three-dimensional random-field Ising model, *Eur. Phys. J. B* **89**, 1 (2016).
- [58] W. H. Press, S. A. Teukolsky, W. T. Vetterling, and B. P. Flannery, *Numerical Recipes: The Art of Scientific Computing*, 3rd ed. (Cambridge University Press, Cambridge, 2007).
- [59] M. Schwartz and A. Soffer, Exact Inequality for Random Systems: Application to Random Fields, *Phys. Rev. Lett.* **55**, 2499 (1985).
- [60] D. S. Fisher, Scaling and Critical Slowing Down in Random-Field Ising Systems, *Phys. Rev. Lett.* **56**, 416 (1986).
- [61] M. Schwartz, The random-field puzzle. I. Solution by equivalent annealing, *J. Phys. C: Solid State Phys.* **18**, 135 (1985).
- [62] M. Schwartz, M. Gofman, and T. Natterman, On the missing scaling relation in random field systems, *Physica A* **178**, 6 (1991).
- [63] M. Schwartz, Breakdown of hyperscaling in random systems—an inequality, *Europhys. Lett.* **15**, 777 (1991).
- [64] G. Grinstein, Ferromagnetic Phase Transitions in Random Fields: The Breakdown of Scaling Laws, *Phys. Rev. Lett.* **37**, 944 (1976).